SLAC-PUB-14660

Elementary steps of syngas reactions on $Mo_2C(001)$: Adsorption thermochemistry and bond dissociation

Andrew J. Medford[a,b], Aleksandra Vojvodic[a,b], Felix Studt[b], Frank Abild-Pedersen[b], Jens K. Nørskov[a,b,*]

[a] *Department of Chemical Engineering, Stanford University, Stanford, California 94305*
[b] *SUNCAT Center for Interface Science and Catalysis, SLAC National Accelerator Laboratory, 2575 Sand Hill Road, Menlo Park, CA 94025, USA*

Abstract

Density functional theory (DFT) and *ab initio* thermodynamics are applied in order to investigate the most stable surface and subsurface terminations of $Mo_2C(001)$ as a function of chemical potential and in the presence of syngas. The Mo-terminated (001) surface is then used as a model surface to evaluate the thermochemistry and energetic barriers for key elementary steps in syngas reactions. Adsorbtion energy scaling relations and Brønsted-Evans-Polanyi relationships are established and used to place Mo_2C into the context of transition metal surfaces. The results indicate that the surface termination is a complex function of reaction conditions and kinetics. It is predicted that the surface will be covered by either C_2H_2 or O depending on conditions. Comparisons to transition metals indicate that the Mo-terminated $Mo_2C(001)$ surface exhibits carbon reactivity similar to transition metals such as Ru and Ir, but is significantly more reactive towards oxygen.

Keywords: carbides, catalysis, synthesis gas, density functional theory, Brønsted-Evans-Polanyi relationships, ab initio thermodynamics

1. Introduction

Reactions involving carbon oxides and hydrocarbons are important for numerous processes including synthetic fuel production, methane reforming, hydrocarbon cracking, and synthesis/isomerization of industrial chemicals [1, 2, 3, 4, 5, 6, 7, 8]. These reactions are traditionally catalyzed with transition metals which often suffer from high cost, poisoning, graphitization, or carburization [1, 9, 3, 2, 10] . The use of transition metal carbides as catalysts presents an interesting alternative due to the possibility of unique Mars-van-Krevelen type mechanisms [11], inherent stability against bulk carburization, and potentially lower costs [3]. Carbide catalysts have been the subject of numerous theoretical and experimental investigations since their activity was compared to platinum by Levy and Boudart [12], and have proven to be active for many different reactions [8, 3, 13].

Molybdenum carbide in particular has shown catalytic activity for conversion of syngas to hydrocarbons and alcohols [14, 15, 16, 17, 18, 19, 20, 8, 21, 22], steam/dry reforming [6, 18, 3, 10, 23, 24, 25], water-gas shift [26, 27, 28], methane aromatization [7, 29, 30], hydrocarbon hydrogenolysis [6, 19, 14, 18], hydrocarbon hydrogenation [8, 31, 32] and various other reactions involving hydrocarbons and alcohols [8, 33, 30, 34, 35]. The activity and selectivity of molybdenum carbide differs depending on the synthesis procedure and reaction conditions [17], and can be tuned using alkali metal promoters such as potassium or rubidium [36, 37]. In order to further improve the performance of molybdenum carbide catalysts it is of value to understand the reactivity, selectivity, and stability of molybdenum carbide under various conditions.

Numerous theoretical studies have investigated the surface stability [38, 39, 40, 41], adsorption energies [42, 43, 44, 45, 46, 47, 48, 49, 50, 51, 40, 52], reaction energetics [53, 54, 46, 55, 52], and alkali-doping [40, 50] on Mo_2C. The most well-studied surface is the $Mo_2C(001)$ surface, and both orthorhombic and hexagonal close packed Mo_2C have been investigated. The results have indicated that the non-polar (011) surface is the most stable regardless of carbon chemical potential, but that the surface energies are sufficiently close that all surfaces are expected to be present on nanoparticles [40, 39].

In this work we seek to provide a more complete view of the energetics of elementary steps in syngas reforming reactions on Mo_2C under relevant conditions. *Ab initio* thermodynamics [56] is employed to provide a consistent framework and allow consideration of the presence of carbon, hydrogen and oxygen. Reaction energies and barriers of various elementary steps are then compared to results from transition metal catalysts in order to provide intuition about the general trends of reactivity on Mo_2C catalysts. The results indicate that carbon reactivity on $Mo_2C(001)$ is similar to group VIII/IX metals, while $Mo_2C(001)$ is slightly more reactive than group VI

*Corresponding Author
Email address: norskov@stanford.edu (Jens K. Nørskov)

Work supported in part by US Department of Energy contract DE-AC02-76SF00515.

metals towards oxygen and hydrogen.

2. Methods

All density functional theory (DFT) calculations are performed with the GPAW code [57], and exchange-correlation interactions are treated by the RPBE functional [58]. A Fermi-Dirac smearing of 0.1 eV was used to achieve convergence, and results were extrapolated to 0 K. A grid spacing of 0.18 Å with a k-point sampling of 4×4×4 (bulk) or 4×4×1 (surface) is used for all calculations. These parameters are found to be sufficient to converge the energy to within 2 meV/atom of the value at 0.1 Å grid spacing and 8×8×8 k-points. Atomic geometries were relaxed using the line-search BFGS algorithm until the maximum force was less than 0.05 eV/atom. Bulk calculations were carried out with a single unit cell with periodic boundaries in all directions. Surface calculations were performed using a 1×1×2 unit cell where the lower (4 layer) unit cell was constrained to the bulk geometry while the upper unit cell was allowed to relax. The surface was modelled using 10 Å of vacuum with no periodic boundary condition in the direction perpendicular to the surface; a dipole correction scheme was included in the Poisson solver. The surface unit cell is shown in Figure 1(a). Kinetic barriers were estimated using a fixed bond length analysis. Thermodynamic quantities were computed using statistical mechanics along with previously developed formalisms. Details are provided in the Appendix.

3. Results and Discussion

3.1. Orthorhombic Mo_2C

3.1.1. Bulk structure

Molybdenum carbide exists in three stable phases at temperatures below 1500 K: orthorhombic Mo_2C at low temperatures, and hexagonal Mo_2C or MoC at higher temperatures [59]. This study focuses on the orthorhombic Mo_2C crystal structure, henceforth abbreviated as simply Mo_2C. The orthorhombic structure consists of Mo atoms distorted slightly from hexagonal positions with carbons inserted into the interstitial sites as shown in Figure 1(a).

The bulk lattice constants were determined to be a=4.839 Å, b=6.173 Å, and c=5.322 Å which are within 2.5% of the experimental values (a=4.72, b=6.01, c=5.20) [59]. The relative stabilities of different carbon positions within the interstitial sites was also investigated. The results confirm the experimentally observed Fe_2N-ζ structure [59] as the most stable. The bulk modulus and formation energy of Mo_2C was also evaluated. The bulk modulus was found to be 282.3 GPa, which is within 10% of the experimental value of 307.5 GPa [60]. The formation energy was found to be -0.21 eV/Mo_2C which should be compared to the experimental value of -0.49 eV/Mo_2C [61]. This large discrepancy, as well as the smaller discrepancies for lattice constants and bulk modulus, are consistent with the known error trends of the RBPE functional for bulk systems [62]. Previous studies of Mo_2C with generalized gradient functionals have resulted in lattice constants within 0.5% [45], bulk modulii within 0.1% [48], and formation energies within 9% [39] of reported experimental values. This indicates that the generalized gradient approximation provides an accurate description of the electronic structure of Mo_2C. The RPBE functional is used for this study since it provides an improved description of the adsorption properties of surfaces [58].

3.1.2. Mo_2C(001) Surface

The surface energies of various hexagonal Mo_2C basal planes have been thoroughly investigated by Shi *et. al.* [39], Han *et. al.* [40], and Wang *et. al.*. All studies have determined that the lowest energy surface is the Mo_2C(011) surface regardless of carbon chemical potential. However, Wulff constructions have shown that the Mo_2C(001) surface is expected to exist on nanoparticles. Han *et. al.* [40] showed that there is no dominant surface for Mo_2C nanoparticles when the carbon chemical potential is below that of graphite since all surface energies were relatively close (2.2-3.4 J/m^2). Wang *et. al.* [41] found that the Mo_2C(001) surface is still present when more reactive carbon is present, although to a lesser extent. No previous studies have investigated the effects of hydrogen or oxygen on surface energies. The Mo_2C(001) surface is chosen as a starting point to investigate effects of hydrogen and oxygen on Mo_2C surface stability since it has a simple structure, is the most close-packed surface, and is predicted to have significant presence on nanostructured Mo_2C [40, 41].

The Mo_2C(001) surface can be either Mo- or C-terminated as shown in the top and bottom surfaces of Figure 1(a). The cleavage energy for the formation of the two surfaces is computed to be 6.12 J/m^2, in good agreement with the value of 5.94 J/m^2 calculated by Han *et. al.* [40]. The Mo-terminated Mo_2C(001) surface is used as the reference point for this work since the surface carbons of the C-terminated surface can participate in reactions and desorb during a catalytic cycle.

The Mo-terminated surface has four unique threefold-hollow sites: one above a lower-layer carbon ($H_{C(l)}$), one above an upper-layer carbon ($H_{C(u)}$), and two sites above Mo atoms - one which exhibits stronger binding ($H_{Mo(s)}$) and one which exhibits weaker binding ($H_{Mo(w)}$) [see Figure 1(b)]. The reactivity of each site was examined for carbon, hydrogen, and oxygen. Each atomic adsorbate followed a similar trend with the $H_{C(l)}$ site showing the highest reactivity in agreement with several previous studies [45, 46, 49, 40]. The specific adsorption energies for carbon and oxygen are shown in Figure 1(c). On-top and bridge sites were also investigated, but were found to be unstable for atomic adsorbates. The trend in reactivity from Figure 1(c) was assumed to be valid for all $C_xH_yO_z$ adsorbates since the trend was valid for carbon, hydrogen, and oxygen adsorption, and molecular adsorption energies

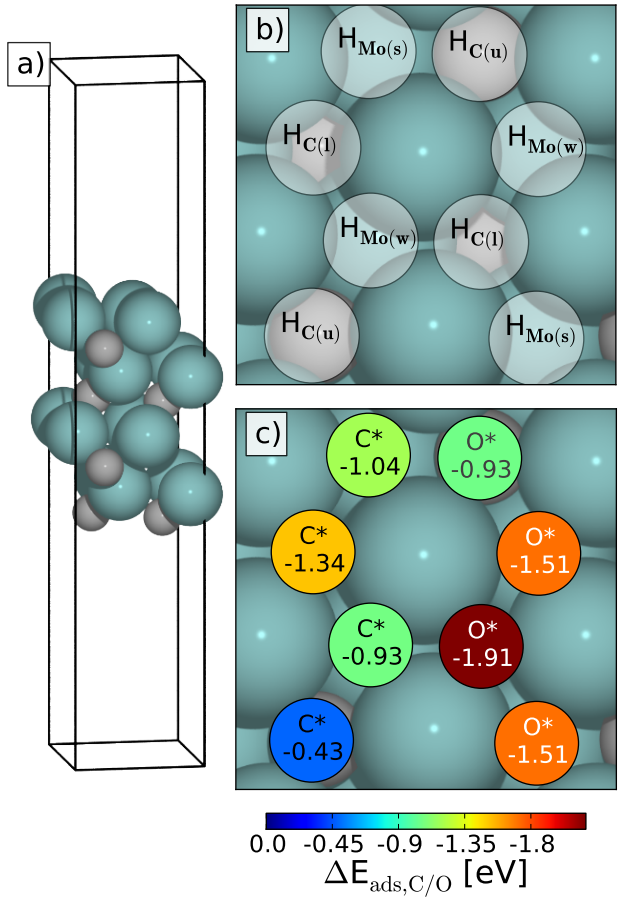

Figure 1: Computational unit cell for $Mo_2C(001)$ (a), definition of adsorption sites on Mo-terminated $Mo_2C(001)$ (b), and relative reactivity towards carbon/oxygen for various surface sites (c). Adsorption energies shown are calculated for carbon and oxygen assuming syngas deposition and water decomposition (see Appendix Section Appendix C). ΔG_{finite} is neglected.

have been previously shown to scale with atomic adsorption energies [63]. Therefore, the $H_{C(l)}$ site was used as an initial position for the relaxation of all $C_xH_yO_z$ adsorbates at 0.25 ML coverage.

3.1.3. $Mo_2C(001)$ Subsurface

Under realistic conditions it is possible that the $Mo_2C(001)$ may form a subsurface oxide, hydride, or oxycarbide. Some experimental reports have indicated the presence of surface oxides or oxycarbides [8, 64, 31], while others have shown no signs of oxygen incorporation [18, 10]. For this reason we have investigated the stability of carbon, hydrogen, and oxygen substitutions, insertions, and vacancies within the first subsurface layer. In order to evaluate subsurface stabilities the surface free energy formalisms outlined in the Appendix were used [56]. The results in Figure 2(a) show the stoichiometry of the most stable first subsurface layer as a function of carbon and oxygen chemical potential. Figure 2(a) indicates that subsurface oxides or oxycarbides will become stable when the chemical potential of oxygen is sufficiently high. This is expected to be the case if oxygen is deposited via CO methanation or O_2 dissociation (see Appendix Equation C.2). The results also indicate that under less agressive oxidizing conditions, such as those present when oxygen is deposited via water or CO_2 decomposition (see Appendix Equation C.2), the subsurface will be stable against oxidation.

All reference energies used assume that oxygen is provided only via an exchange with the gas-phase. In reality many Mo_2C catalysts are prepared by carburizing a MoO_x precursor [18, 7]. Oxygen is also ubiquitous in most environments, and it has been hypothesized that gaseous oxygen can diffuse into bulk Mo_2C [18]. The presence of oxygen in the bulk lattice would provide an additional reservoir for subsurface oxygen. This could significantly change the relevant oxygen chemical potential; however, the nature of this effect would be synthesis dependent and is outside the scope of this work.

Figure 2 also indicates that both carbon vacancies and insertions will become stable depending on the carbon chemical potential. The chemical potentials necessary to form carbon vacancies are very unlikely to occur under syngas reaction conditions since CO is a reactive carbon source. Subsurface carbon insertions are also considered unlikely. Carbon is more stable adsorbed on top of the surface than when inserted into the subsurface. For this reason the C-terminated $Mo_2C(001)$ surface would be more stable than subsurface carbon insertions.

In order to improve intuition about the surface stabilities the chemical potentials of carbon, hydrogen, and oxygen were explicitly computed as a function of temperature and pressure (see Appendix Section Appendix A). Such an analysis requires knowledge of the deposition reactions and gas composition. We have shown the results of several assumed deposition reactions and gas compositions in Figure 2(b-d). The compositions correspond to a syngas feedstock with an initial composition of around

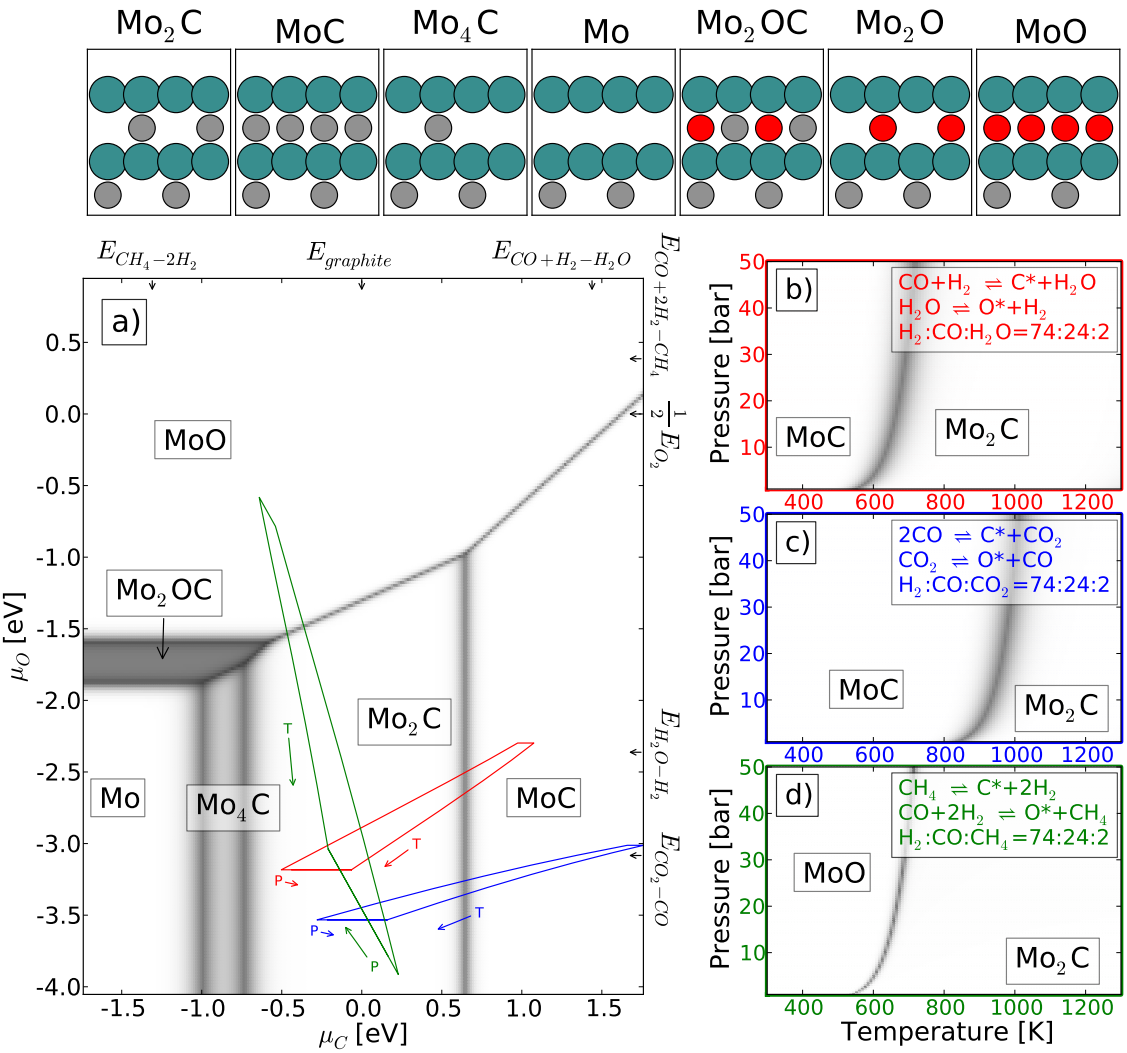

Figure 2: Thermodynamic stability of various Mo-terminated Mo_2C(001) subsurfaces (schematics at top of figure) as a function of carbon and oxygen chemical potential assuming a static μ_H(600 K, 1 bar) (a). Surface phase diagrams as a function of temperature and pressure assuming carbon, hydrogen, and oxygen are deposited via several reactions and gas compositions (b-d). Hydrogen is always deposited via dissociative adsorption. Carbon/oxygen deposition reactions and gas compositions are indicated in the figure. Relevant chemical potentials for (b-d) are projected onto the $\mu_C - \mu_O$ plane by the corresponding colored boxes in (a). DFT energies of some relevent references are indicated by arrows in (a). Shading represents relative coverage of one unit cell of the lowest energy surface according to the Boltzmann distribution at T=600 K (white=1, black=0). ΔG_{finite} and U_{ZPE} were neglected for subsurfaces.

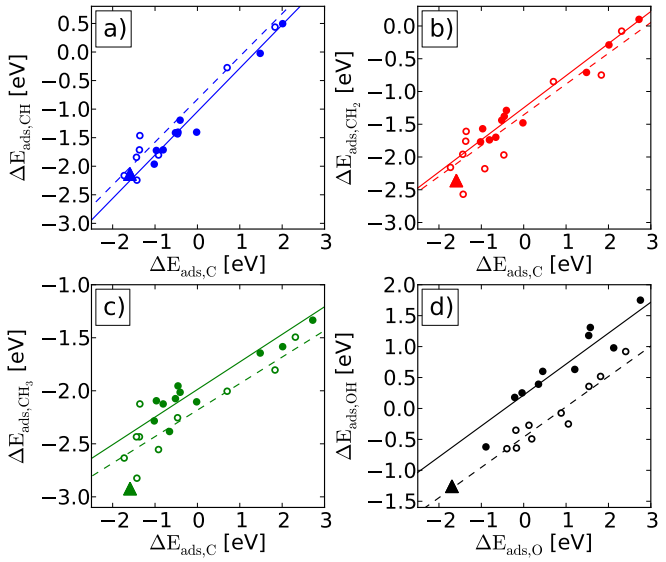

Figure 3: Adsorption scaling shows linear relationship between C/CH_x adsorption energies (a-c) and O/OH_x adsorption energies (d). Solid lines/solid circles indicate metal (111) scaling, and dashed lines/hollow circles indicate metal (211) scaling. Solid triangles represent adsorption at the $H_{C(l)}$ site of Mo-terminated $Mo_2C(001)$. Carbon and oxygen are referenced to syngas deposition and water decomposition (see Appendix Section Appendix C). Lines have mean average errors on the order of 0.1 eV (Modified from [63]). All zero-point and thermal corrections are neglected.

3:1 H_2:CO with a low conversion to the relevant product (74:24:2 H_2:CO:product). The results are found to depend on the choice of carbon and oxygen deposition reactions (See Appendix Equations C.2 and C.3). When oxygen is deposited from water or carbon dioxide decomposition the Mo_2C surface is stable against subsurface oxidation. If oxygen is deposited from CO methanation a subsurface oxycarbide is predicted to be stable at low temperatures. The kinetics of CO methanation are expected to be slower than decomposition of water or carbon dioxide, therefore the stoichiometric Mo_2C surface is expected to be stable under most syngas reaction conditions. For this reason the Mo-terminated $Mo_2C(001)$ subsurface is chosen as the base surface for subsequent calculations.

3.2. Adsorption Thermochemistry

3.2.1. $C_xH_yO_z$ Adsorption Energies

The reactivity of the Mo-terminated $Mo_2C(001)$ surface towards various hydrocarbon and alcohol intermediates is shown in Table 1. The adsorption energies are calculated using Equation C.4 (T=0 K) and reference energies assuming water decomposition and syngas deposition (see Equations C.2 and C.3). Table 1 indicates several important trends amongst various intermediates. First, alcohol intermediates exhibit lower binding energies in general, which could explain the observation that Mo_2C is selective towards hydrocarbons. Secondly, hydrogenation of most carbon-containing species is thermodynamically favorable, providing a driving force for converting carbon species into hydrocarbons or alcohols; however, hydrogenation of O* and OH* is thermodynamically uphill, which indicates that the surface is susceptible to a buildup of adsorbed oxygen.

Previous work on transition metals has revealed a linear correlation between the binding energies of C and CH_x as well as O and OH_x [63]. These scaling relations can be used to examine how adsorption to $Mo_2C(001)$ $H_{C(l)}$ site compares to adsorption on metal surfaces. The adsorption energies of CH_x and OH_x species were compared with transition metal (211) [M(211)] and (111) [M(111)] surfaces. Figure 3(a) indicates that Mo_2C is most similar to the M(211) surfaces, and is slightly more reactive towards $CH_{2/3}$ species than metals with comparable carbon adsorption strengths. This indicates that Mo_2C should be a favorable catalyst for hydrogenation reactions and may be less susceptible to graphite poisoning due to an increased affinity towards hydrocarbons. Figure 3(b) shows that O/OH_x binding on $Mo_2C(001)$ is similar to binding on M(211) surfaces. It can also be seen that Mo_2C is highly reactive towards oxygen, which indicates that oxygen poisoning may be an issue on Mo_2C surfaces.

3.2.2. CH_x and OH_x coverages

The thermodynamics of chemisorption under reaction conditions will determine the equilibrium surface coverages of various adsorbates. Surface free energies of adsorbates at various coverages were evaluated using the surface free energy formalism (see Appendix Section Appendix B). For this analysis the energy of H, CO, CH_x, and OH_x species adsorbed at 0.25, 0.5, 0.75, and 1 ML on the Mo-terminated $Mo_2C(001)$ surface was calculated explicitly. First, $CH_{x<3}$ species were adsorbed at the $H_{C(l)}$ sites. Additional $CH_{x<3}$ species were most stable when adsorbed at the $H_{Mo(s)}$ sites. This resulted in spontaneous coupling of the $CH_{x<3}$ adsorbates to form adsorbed C_2H_{2x}. Spontaneous coupling was only observed when the two species began in adjacent adsorption sites (e.g. $H_{C(l)}/H_{Mo(s)}$ or $H_{C(u)}/H_{Mo(w)}$). At high coverages C_2H_{2x} formation is thermodynamically favorable, and spontaneous coupling between adjacent sites indicates that it will also be kinetically facile. This attractive interaction between $CH_{x<3}$ species is unusual; most surface adsorbates exhibit repulsive interactions [40, 65], and carbon coupling is often activated even for adjacent adsorption sites [65, 66]. This propensity towards coupled carbons is consistent with the activity of Mo_2C for methane aromatization [7] and Fischer-Tropsch synthesis [15, 16, 17, 22].

In the case of H, CO, CH_3 and OH_x species the adsorbates were also first adsorbed at the $H_{C(l)}$ sites for coverages of 0.25/0.5 ML. The most stable adsorption at 0.75/1.0 ML was found to occur via the $H_{C(u)}$ sites. This behavior is attributed to strong adsorbate-adsorbate repulsions between these adsorbates.

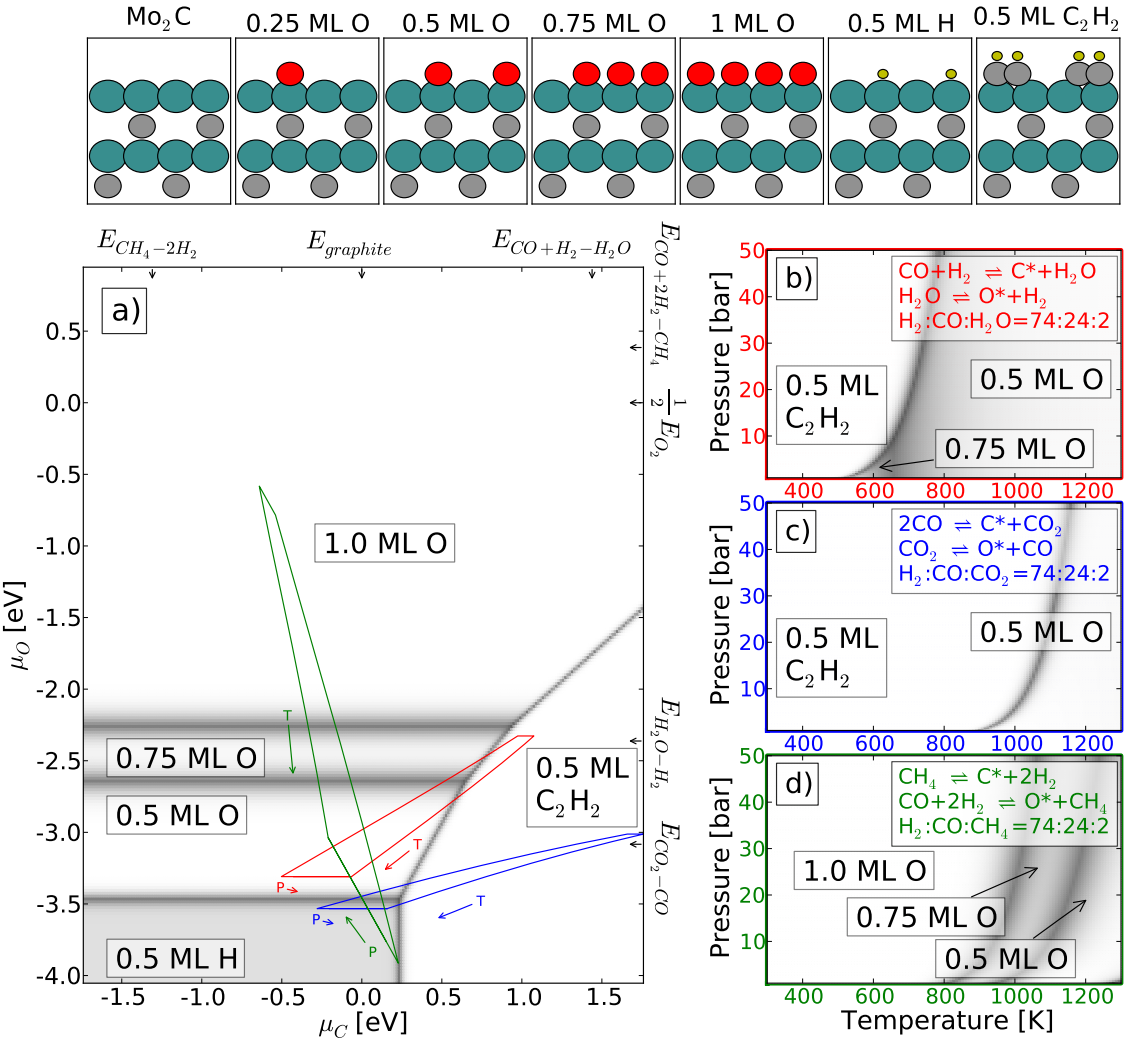

Figure 4: Thermodynamic stability of various $CO/CH_x/OH_x$ surface coverages (schematics at top of figure) on Mo-terminated $Mo_2C(001)$ surface as a function of carbon and oxygen chemical potential assuming a static $\mu_H(600\ K, 1\ bar)$ (a). Surface phase diagrams as a function of temperature and pressure assuming carbon, hydrogen, and oxygen are deposited via several reactions and gas compositions (b-d). Hydrogen is always deposited via dissociative adsorption. Carbon/oxygen deposition reactions and gas compositions are indicated in the figure. Relevant chemical potentials for (b-d) are projected onto the $\mu_C - \mu_O$ plane by the corresponding colored boxes in (a). DFT energies of some relevent references are indicated by arrows in (a). Shading represents relative coverage of one unit cell of the lowest energy surface according to the Boltzmann distribution at T=600 K (white=1, black=0).

		C_xH_y				C_xH_yO	
n_C	n_H	Adsorbate	ΔE_{ads} [eV]	n_C	n_H	Adsorbate	ΔE_{ads} [eV]
0	1	H*	-0.755	0	0	O*	-1.908
1	0	C*	-1.335	0	1	OH*	-1.267
1	1	CH*	-1.72	0	2	H_2O*	-0.058
1	2	CH_2*	-1.78	1	0	CO*	-1.851
1	3	CH_3*	-2.144	1	1	HCO*	-1.482
2	0	CC*	-2.749	1	2	CH_2O*	-1.712
2	1	CCH*	-3.128	1	3	CH_3O*	-2.093
2	2	CHCH*	-3.394	2	0	CCO*	-2.54
2	3	$CHCH_2$*	-2.75	2	1	CHCO*	-3.171
2	4	CH_2CH_2*	-2.952	2	2	CHCHO*	-3.068
2	5	CH_2CH_3*	-3.109	2	3	CH_3CO*	-3.236
				2	4	CH_3CHO*	-2.996

Table 1: Binding energies of C_xH_y and C_xH_yO at the $H_{C(l)}$ adsorption site. Carbon and oxygen references are syngas deposition and water decomposition (see Appendix Section Appendix C). ΔG_{finite} is neglected.

Figure 4(a) shows the predicted surface terminations as a function of carbon and oxygen chemical potential for various adsorbate coverages. It is found that the dominant surface species will depend upon the source of both carbon and oxygen. The surface energies were explicitly calculated under some specific reaction conditions, similar to the previous analysis for subsurfaces. The results are shown in Figure 4(b-d). Under the considered conditions there are two regimes: hydrocarbon (C_xH_{2x}) terminated and oxygen terminated surfaces. The hydrocarbon termination is dominant at low temperatures with a reactive carbon source such as CO, and the oxygen termination is dominant at high temperatures or with a stable carbon source such as CH_4. These results suggest that the most relevant $Mo_2C(001)$ surface to use for studying syngas reactions is the oxygen passivated surface or hydrocarbon terminated surface. Previous work has suggested that the oxygen passivated surface may temper the high reactivity of the Mo-terminated $Mo_2C(001)$ surface, leading to improved catalytic activity [52]. Adsorbed oxygen, carbon, or hydrocarbons can desorb as part of catalytic cycles, therefore the termination will depend on both thermodynamic conditions and reaction kinetics. The Mo-terminated surface is well-defined since its composition will not change during a reaction, and it represents the most reactive state of $Mo_2C(001)$. For this reason Mo-terminated $Mo_2C(001)$ surface is a good starting point for understanding the reactivity of Mo_2C, and is the focus of the remainder of this study. The surface coverage analysis conducted here does not include the possibility of mixed adsorption between H, CH_x and OH_x species, or the formation of species containing more than two carbons. Furthermore, only the Mo-terminated $Mo_2C(001)$ surface with coverages between 0.25 and 1 ML are considered. Despite this, the analysis provides insight into the competition between hydrocarbon and oxygen adsorption on Mo_2C and reveals that the C-terminated $Mo_2C(001)$ surface which has been previously studied is not expected to be stable under realistic conditions since carbon dimerization and hydrogenation are both thermodynamically favorable.

3.3. Bond dissociation energetics

The kinetics of reactions depend upon the energetic barriers of elementary steps. Brønsted-Evans-Polanyi (BEP) relationships provide a useful framework for relating the thermodynamic driving force and the transition-state energy of dissociation reactions. BEP relations were originally conceived [67, 68] as a relationship between the reaction energy (ΔE_{rxn}) and the activation energy (ΔE_a) as shown schematically in Figure 5.

Dissociation and coupling of carbon and oxygen species plays an important role in the reactivity and selectivity of syngas conversion reactions. Hydrogen assisted dissociation of CO is the rate-limiting step for methane synthesis on Ni [69], and barriers for carbon-carbon coupling determine the mechanism and average chain length in Fischer-Tropsch synthesis [66]. Thus, the energy barriers for these types of elementary reactions on $Mo_2C(001)$ provide important information about the catalytic activity of the surface.

The reaction energies and energetic barriers for CH_x-O (C-O) dissociation are given in Figure 6(a). The activation energy of CO dissociation is relatively low (1.43 eV) compared to active transition metal catalysts such as Ni (2.10 eV) [9]. It also interesting that hydrogenation of CO leads to significantly lower CO dissociation barriers. This suggests that CO dissociation may occur via a hydrogenated intermediate on Mo_2C, and could also explain the low selectivity towards alcohols [21, 4]. The energetics of CH_x-CH_x (C-C) and some CH_x-CH_yO (C-CO) coupling reactions are shown for Mo-terminated $Mo_2C(001)$ in Figure 6(b). All coupling barriers are below 1.5 eV, and many are below 1 eV which suggests that carbon-carbon coupling is kinetically facile on Mo-terminated $Mo_2C(001)$. The

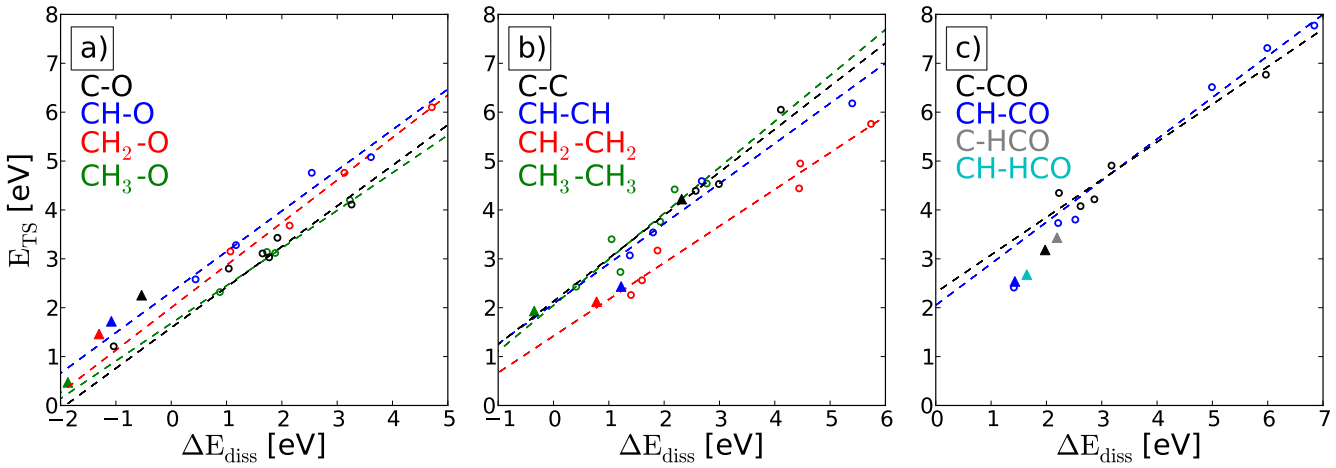

Figure 7: Comparison of C-O (a), C-C (b), and C-CO (c) dissociation energetics on $Mo_2C(001)$ (solid △) and various transition metals (hollow ○). M(211) BEP lines from Ref [70] are shown for comparison. The dissociation and transition-state adsorption energies are calculated with Equations 1 and 2 respectively where the C/H/O references are methane cracking, hydrogen dissociation, and water decomposition (see Appendix Section Appendix C).

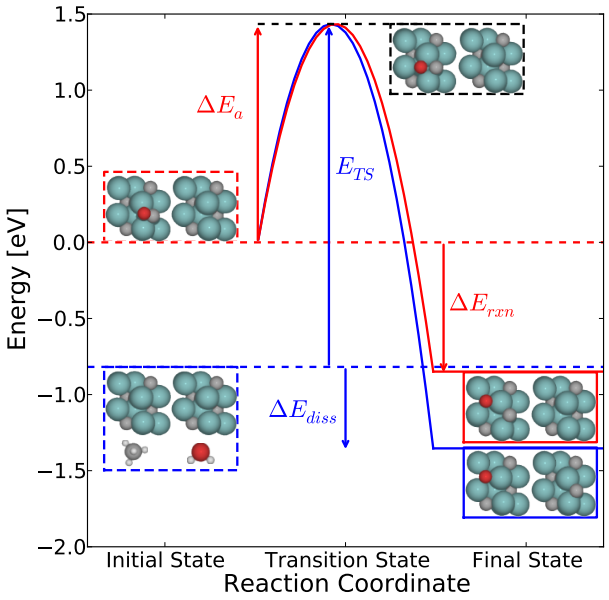

Figure 5: Schematic showing the definition of ΔE_a, ΔE_{rxn}, E_{TS}, and ΔE_{diss} for the case of CO dissociation. Images represent the DFT energy of the depicted atoms. The CH_4 molecule refers to C from metane cracking (Equation C.3) and the H_2O molecule refers to O from water decomposition (Equation C.2).

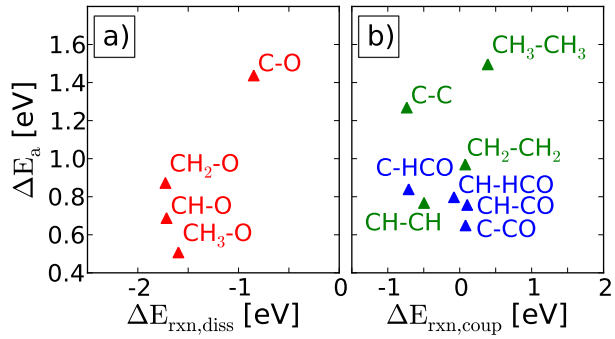

Figure 6: Reaction and activation energies for CH_x-O (red) dissociation (a) and CH_x-CH_x/CH_x-H_yCO (green/blue)

fact that couplings involving HCO are more favorable than most CH_x couplings supports the hypothesis that Fischer-Tropsch type reactons occur via the oxygenate mechanism on Mo_2C [71]. The particularly low barrier for CH-CH couplings is supported by the activity of molybdenum carbide for methane aromitization [7, 29].

For the purpose of microkinetic modeling and comparison with previous work, it is useful to also consider the BEP relationship between the adsorption energy of the dissociated species (ΔE_{diss}) and the transition-state referenced to the gas-phase (E_{TS}) as given by Equation 1 and 2 respectively.

$$\Delta E_{diss} = \Delta E_{ads,A} + \Delta E_{ads,B} \quad (1)$$

$$E_{TS} = E_{A-B^{\ddagger}} - E_{Mo_2C} - E_{A_{gas}} - E_{B_{gas}} \quad (2)$$

where $\Delta E_{ads,X}$ is the adsorption energy of X at the $H_{C(l)}$ site, $E_{A-B^{\ddagger}}$ is the transition-state DFT energy of A-B dissociation, E_{Mo_2C} is the energy of a Mo-terminated $Mo_2C(001)$ slab, and $E_{X_{gas}}$ is the gas-phase reference energy of X. Oxygen and carbon gas-phase energies are based on water decomposition and methane cracking (Equations C.2a and C.3a). All zero-point contributions are neglected. This set of definitions allows direct comparison with previously published BEP relations for M(211) surfaces [70] and is shown schematically in Figure 5. Comparison to (211) step sites is relevant since these undercoordinated surfaces are often considered to be the active site for catalysis on transition metals [72]. Furthermore, adsorption on the $Mo_2C(001)$ $H_{C(l)}$ site is most simliar to adsorbate scaling relations for M(211) sites (Figure 3).

Using the BEP relations between adsorption of dissociated species and the transition-state energy, it is possible to place the thermodynamics and kinetics of elementary steps on $Mo_2C(001)$ into the context of transition metal catalysts. Mo-terminated $Mo_2C(001)$ is compared to previously determined adsorption BEP relations for M(211)

surfaces [70] in Figure 7. The transition-state energies of C-O dissociation reactions [Figure 7(a)] are slightly higher compared to BEP relations for M(211) surfaces. However, the dissociation of C-O bonds is more thermodynamically favorable on $Mo_2C(001)$ than on the transition metals included in this comparison. The BEP relations from Figure 7 are assumed to be valid in the range where the transition-state resembles the product [70], so it is unsurprising that the exothermic C-O dissociations on Mo-terminated $Mo_2C(001)$ deviate from the BEP lines [73].

Transition-state energies for C-C dissociation on Mo-terminated $Mo_2C(001)$ are similar to transition metals with comparable dissociation energies [Figure 7(b)]. This is a consequence of the fact that carbon and CH_x binding energies are similar to late transition metals, as shown in Figure 3(a). Figure 7(c) shows that the transition-state energies of C-CO dissociations are slightly lower compared to the BEP lines for transition metals. Low barriers for C-CO dissociations could explain the relatively low average chain length of higher hydrocarbons and alcohols obseved from syngas conversion over Mo_2C. If chain propagation occurs via an oxygenate mechanism then the low transition-state energy of the activated C-CO complex would lead to a competition between coupling and dissociation of carbon-carbon bonds.

3.4. Comparison to Transition Metals

The idea that carbides are less reactive than their transition metal counterparts was suggested by Levy and Boudart in their comparison of tungsten carbide and platinum [12]. Since then Mo_2C has been compared to Ru [12, 14, 19] and Ir [3] for CO hydrogenation and methane reforming. The binding energies of carbon, oxygen, and hydrogen are displayed as scatter plots for various M(211) surfaces along with $Mo_2C(001)$ in Figure 8. Figure 8 suggests that the chemistry of carbon on Mo-terminated $Mo_2C(001)$ is indeed similar to Ru and Ir, as well as Fe, Co, Rh, Ni and Pd. The fact C/CH_x binding on $Mo_2C(001)$ is similar to the M(211) C/CH_x adsorbate scaling relations [Figure 3(a)] indicates that Mo_2C should exhibit similar activity to these metals for reactions where hydrocarbons are the main intermediates.

It is also found that the Mo-terminated $Mo_2C(001)$ surface exhibits a unique decoupling of carbon and oxygen/hydrogen chemistries as compared to transition metals. Figure 8(a) shows that $Mo_2C(001)$ is much more reactive towards oxygen than transition metals with similar carbon binding energies, and actually binds oxygen stronger than metallic molybdenum. Even as the oxygen surface coverage is increased, $Mo_2C(001)$ binds oxygen more strongly than transition metals with comparable carbon binding energies. Figure 8(b) shows a similar trend for hydrogen binding, although the absolute differences between $Mo_2C(001)$ and transition metals are much smaller than for the oxygen case since hydrogen binding energies vary much less even across transition metals. It is interesting to note that $Mo_2C(001)$ is most similar to Ir in the carbon/hydrogen scatter plot, and Ir has been directly compared to Mo_2C for steam reforming [3].

The results of this analysis indicate that the comparison between the activity of Mo_2C and transition metals such as Ru and Ir is an oversimplification. The reactivity of Mo_2C is dependent upon reactant composition and reaction conditions. In reactions where the primary intermediates are adsorbed hydrocarbons, Mo_2C may produce reactivity/selectivity patterns similar to Ru, Ir, Fe, Co, or other late transition metals; however, when oxygen is a key intermediate then Mo_2C is likely to exhibit behavior more similar to W or Re. This is supported by the rapid oxidation of Mo_2C oxygen reduction electrocatalysts [74]. The decoupling of carbon and oxygen chemistry separates Mo_2C from transition metals. The behavior suggests that Mo_2C catalysts could exhibit unique activity and selectivity patterns, but that the surface is also more susceptible to oxygen poisoning.

4. Conclusion

Understanding Mo_2C and other carbide materials under reaction conditions is not straightforward and requires consideration of environmental carbon, oxygen, hydrogen, and any other elements present. The formalism of *ab initio* thermodynamics provides a framework for conducting such analyses. Thermodynamic conditions will change as a function of time and space within a reactor, and are therefore ill-defined in realistic scenarios. By making assumptions regarding these unknowns it was shown that $Mo_2C(001)$ is predicted to be terminated with hydrocarbons or oxygen under syngas reaction conditions. It was also found that carbon-carbon coupling becomes spontaneous at CH_x coverages greater than 0.5 ML. These findings are consistent with the activity of Mo_2C for conversion of syngas to light hydrocarbons, and indicate that Mo_2C is a possible candidate for Fischer-Tropsch catalysis.

It was also shown that the hydrocarbon reactivity of Mo-terminated $Mo_2C(001)$ is similar to Ru, Ir, Fe, Co, Rh, Ni, and Pd; however, Mo-terminated $Mo_2C(001)$ was found to be significantly more reactive towards oxygen and hydrogen. This decoupling distinguishes Mo-terminated $Mo_2C(001)$ from transition metals, and implies that comparisons between carbides and transition metals are only valid under certain reaction conditions. Furthermore, the unique carbon and oxygen chemistry of Mo-terminated $Mo_2C(001)$ could lead to novel reaction mechanisms for syngas reactions.

A further understanding of syngas reactions on Mo_2C will require a comparison of kinetics for specific reaction mechanisms. This work provides a platform for such analyses. In the future, mechanistic models can be constructed and used to explain specific phenomena which currently hinder the widespread use of Mo_2C catalysts such as low alcohol selectivity, deactivation due to oxidation/graphitization, and the formation of only short hydrocarbon chains. By understanding the origin of such issues it may be possible

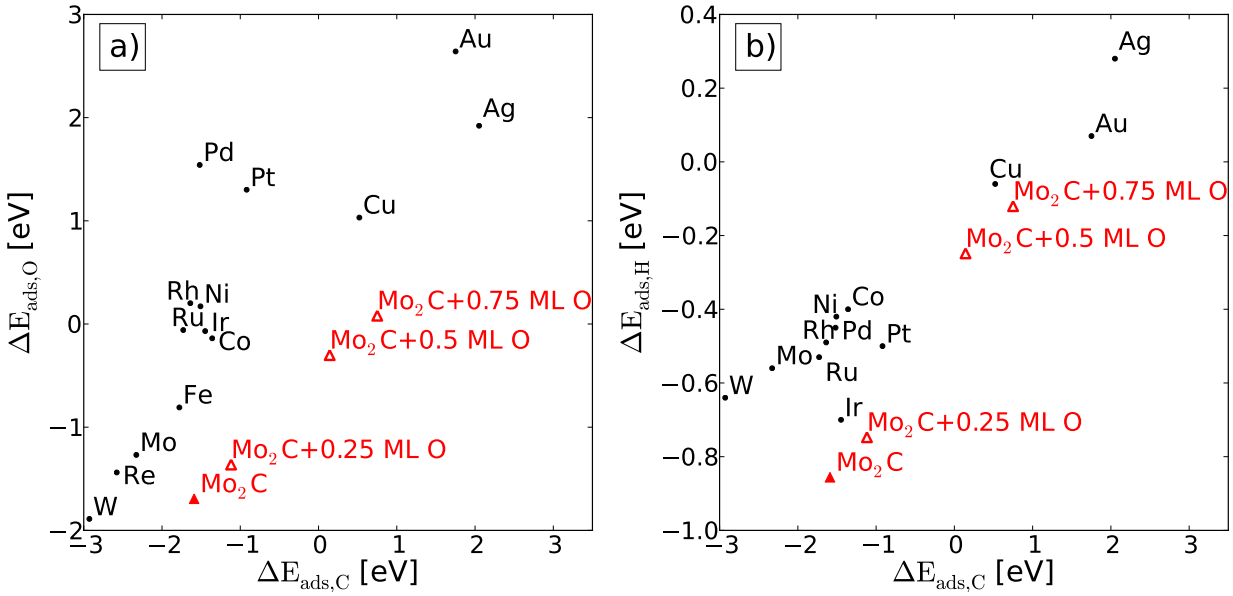

Figure 8: Scatter plot of carbon/oxygen (a) and carbon/hydrogen (b) binding energies for transition metals (black ○), Mo-terminated Mo_2C (red solid △), and Mo_2C with various coverages of oxygen (red hollow △). Adsorption energies for M(211) surfaces are taken from [63]. Carbon and oxygen references are syngas deposition and water decomposition respectively (see Appendix Section Appendix C).

to improve the performance of Mo_2C and other carbide catalysts.

Acknowledgements

This material is based upon work supported by the National Science Foundation Graduate Research Fellowship under Grant No. DGE-1147470. All authors wish to acknowledge support from the U.S. Department of Energy, Office of Basic Energy Sciences. A.V. acknowledges support from the Swedish Research Council.

References

[1] J. R. Rostrup-Nielsen, J. Sehested, J. K. Nørskov, Hydrogen and Synthesis Gas by Steam- and CO2 Reforming, Advances in Catalysis 47 (2002) 65–139. doi:10.1002/chin.200317288.

[2] M. A. Pena, J. Gómez, J. Fierro, New catalytic routes for syngas and hydrogen production, Applied Catalysis A: General 144 (1-2) (1996) 7–57. doi:10.1016/0926-860X(96)00108-1.

[3] J. B. Claridge, New Catalysts for the Conversion of Methane to Synthesis Gas: Molybdenum and Tungsten Carbide, Journal of Catalysis 180 (1) (1998) 85–100. doi:10.1006/jcat.1998.2260.

[4] K. Fang, D. Li, M. Lin, M. Xiang, W. Wei, Y. Sun, A short review of heterogeneous catalytic process for mixed alcohols synthesis via syngas, Catalysis Today 147 (2) (2009) 133–138. doi:10.1016/j.cattod.2009.01.038.

[5] A. M. Saib, D. J. Moodley, I. M. Ciobîc, M. M. Hauman, B. H. Sigwebela, C. J. Weststrate, J. W. Niemantsverdriet, J. van de Loosdrecht, Fundamental understanding of deactivation and regeneration of cobalt FischerTropsch synthesis catalysts, Catalysis Today 154 (3-4) (2010) 271–282. doi:10.1016/j.cattod.2010.02.008.

[6] J. H. Sinfelt, D. J. C. Yates, Effect of Carbiding on the Hydrogenolysis Activity of Molybdenum, Nature Physical Science 229.

[7] F. Solymosi, A. Szske, Conversion of methane to benzene over Mo2C and Mo2C/ZSM-5 catalysts, Catalysis Letters 39 (1996) 157–161.

[8] S. T. Oyama, Preparation and catalytic properties of transition metal carbides and nitrides, Catalysis Today 15 (2) (1992) 179–200. doi:10.1016/0920-5861(92)80175-M.

[9] H. Bengaard, J. K. Nørskov, J. Sehested, B. Clausen, L. P. Nielsen, A. M. Molenbroek, J. Rostrup-Nielsen, Steam Reforming and Graphite Formation on Ni Catalysts, Journal of Catalysis 209 (2) (2002) 365–384. doi:10.1006/jcat.2002.3579.

[10] A. J. Brungs, A. P. E. York, J. B. Claridge, C. M, M. L. H. Green, C. Marquez-Alvarez, Dry reforming of methane to synthesis gas over supported molybdenum carbide catalysts, Catalysis Letters 70 (2000) 117–122.

[11] J. M. Gracia, F. F. Prinsloo, J. W. Niemantsverdriet, Mars-van Krevelen-like Mechanism of CO Hydrogenation on an Iron Carbide Surface, Catalysis Letters 133 (3-4) (2009) 257–261. doi:10.1007/s10562-009-0179-5.

[12] R. B. Levy, M. Boudart, Platinum-like behavior of tungsten carbide in surface catalysis., Science 181 (4099) (1973) 547–9. doi:10.1126/science.181.4099.547.

[13] A.-M. Alexander, J. S. J. Hargreaves, Alternative catalytic materials: carbides, nitrides, phosphides and amorphous boron alloys., Chemical Society reviews 39 (11) (2010) 4388–401. doi:10.1039/b916787k.

[14] L. Leclercq, K. Imura, S. Yoshida, T. Barbee, M. Boudart, Synthesis of New Catalytic Materials: Metal Carbides of the Group VI B Elements, Studies in Surface Science and Catalysis 3 (1979) 627–639. doi:10.1016/S0167-2991(09)60240-8.

[15] I. Kojima, E. Miyazaki, I. Yasumori, Synthesis of Hydrocarbons from CO and H2 over Metal Carbide Catalysts, Journal of the Chemical Society. Chemical Communications 12 (1980) 573.

[16] M. Saito, R. B. Anderson, The Activity of Several Molybdenum Compounds for the Methanation of CO, Journal of Catalysis 446 (1980) 438–446.

[17] J. W. Dun, E. Gulari, K. Y. S. Ng, Fischer-Tropsch synthesis on charcoal-supported molybdenum: The effect of preparation conditions and potassium promotion on activity and selectivity, Applied Catalysis 15 (1985) 247–263.

[18] G. Ranhotra, A. T. Bell, J. A. Reimer, Catalysis over Molybdenum Carbides and Nitrides II: Studies of CO Hydrogenation and C2H6 Hydrogenolysis, Journal of Catalysis 49 (1987) 40–49.

[19] J. S. Lee, M. H. Yeom, D. S. Lee, Catalysis by Molybdenum Carbide in Activation of C-C, C-O and C-H bonds, Journal of Molecular Catalysis 62 (3) (1990) L45–L51. doi:10.1016/0304-5102(90)85219-8.

[20] K. Y. Park, W. K. Seo, J. S. Lee, Selective synthesis of light olefins from syngas over potassium-promoted molybdenum carbide catalysts, Catalysis Letters 11 (3-6) (1991) 349–356. doi:10.1007/BF00764327.

[21] A. Griboval-Constant, J.-M. Giraudon, G. Leclercq, L. Leclercq, Catalytic behaviour of cobalt or ruthenium supported molybdenum carbide catalysts for FT reaction, Applied Catalysis A: General 260 (1) (2004) 35–45. doi:10.1016/j.apcata.2003.10.031.

[22] D.-V. N. Vo, A. A. Adesina, FischerTropsch synthesis over alumina-supported molybdenum carbide catalyst, Applied Catalysis A: General 399 (1-2) (2011) 221–232. doi:10.1016/j.apcata.2011.04.003.

[23] K. Oshikawa, M. Nagai, S. Omi, Characterization of Molybdenum Carbides for Methane Reforming by TPR, XRD, and XPS, Journal of Physical Chemistry B 105 (38) (2001) 9124–9131. doi:10.1021/jp0111867.

[24] R. Barthos, A. Széchenyi, A. Koós, F. Solymosi, The decomposition of ethanol over Mo2C/carbon catalysts, Applied Catalysis A: General 327 (1) (2007) 95–105. doi:10.1016/j.apcata.2007.03.040.

[25] O. Marinflores, S. Ha, Study of the performance of Mo2C for iso-octane steam reforming, Catalysis Today 136 (3-4) (2008) 235–242. doi:10.1016/j.cattod.2008.02.004.

[26] E. Rebrov, S. Kuznetsov, M. Decroon, J. Schouten, Study of the water-gas shift reaction on Mo2C/Mo catalytic coatings for application in microstructured fuel processors, Catalysis Today 125 (1-2) (2007) 88–96. doi:10.1016/j.cattod.2007.01.075.

[27] A. R. Dubrovskiy, S. A. Kuznetsov, E. V. Rebrov, J. C. Schouten, V. T. Kalinnikov, Synthesis of Mo2C coatings by simultaneous electroreduction of MoO 4 2 and CO 3 2 ions in molten salts and their catalytic activity for the water-gas shift reaction, Doklady Chemistry 421 (2) (2008) 186–189. doi:10.1134/S0012500808080053.

[28] T. Namiki, S. Yamashita, H. Tominaga, M. Nagai, Dissociation of CO and H2O during watergas shift reaction on carburized Mo/Al2O3 catalyst, Applied Catalysis A: General 398 (1-2) (2011) 155–160. doi:10.1016/j.apcata.2011.03.029.

[29] F. Solymosi, Aromatization of Methane over Supported and Unsupported Mo-Based Catalysts, Journal of Catalysis 165 (2) (1997) 150–161. doi:10.1006/jcat.1997.1478.

[30] M. Siaj, H. Oudghiri-Hassani, C. Maltais, P. H. McBreen, Thermally Stable Alkylidene Groups on the Surface of β-Mo2C: Relevance to Methane Aromatization and Olefin-Metathesis Catalysis, Journal of Physical Chemistry C 111 (4) (2007) 1725–1732. doi:10.1021/jp064599m.

[31] T.-c. Xiao, A. P. E. York, V. C. Williams, H. Al-Megren, A. Hanif, X.-y. Zhou, M. L. H. Green, Preparation of Molybdenum Carbides Using Butane and Their Catalytic Performance, Chemistry of Materials 12 (12) (2000) 3896–3905. doi:10.1021/cm001157t.

[32] M.-L. Frauwallner, F. López-Linares, J. Lara-Romero, C. E. Scott, V. Ali, E. Hernández, P. Pereira-Almao, Toluene hydrogenation at low temperature using a molybdenum carbide catalyst, Applied Catalysis A: General 394 (1-2) (2011) 62–70. doi:10.1016/j.apcata.2010.12.024.

[33] P. Liu, J. A. Rodriguez, J. T. Muckerman, Desulfurization of SO 2 and Thiophene on Surfaces and Nanoparticles of Molybdenum Carbide: Unexpected Ligand and Steric Effects, Journal of Physical Chemistry B 108 (40) (2004) 15662–15670. doi:10.1021/jp040267a.

[34] N. Ji, T. Zhang, M. Zheng, A. Wang, H. Wang, X. Wang, Y. Shu, A. L. Stottlemyer, J. G. Chen, Catalytic conversion of cellulose into ethylene glycol over supported carbide catalysts, Catalysis Today 147 (2) (2009) 77–85. doi:10.1016/j.cattod.2009.03.012.

[35] D. W. Flaherty, S. P. Berglund, C. B. Mullins, Selective decomposition of formic acid on molybdenum carbide: A new reaction pathway, Journal of Catalysis 269 (1) (2010) 33–43. doi:10.1016/j.jcat.2009.10.012.

[36] H. C. Woo, K. Y. Park, Y. G. Kim, I.-S. Nam, J. S. Chung, J. S. Lee, Mixed alcohol synthesis from carbon monoxide and dihydrogen over potassium-promoted molybdenum carbide catalysts, Applied Catalysis 75 (1) (1991) 267–280. doi:10.1016/S0166-9834(00)83136-X.

[37] H. Shou, R. J. Davis, Reactivity and in situ X-ray absorption spectroscopy of Rb-promoted Mo2C/MgO catalysts for higher alcohol synthesis, Journal of Catalysis 282 (1) (2011) 83–93. doi:10.1016/j.jcat.2011.05.028.

[38] H. Liu, B. Yi, M. Hou, J. Wu, Z. Hou, H. Zhang, Composite Electrode for Unitized Regenerative Proton Exchange Membrane Fuel Cell with Improved Cycle Life, Electrochemical and Solid-State Letters 7 (3) (2004) A56. doi:10.1149/1.1645351.

[39] X.-R. Shi, S.-G. Wang, H. Wang, C.-M. Deng, Z. Qin, J. Wang, Structure and stability of β-Mo2C bulk and surfaces: A density functional theory study, Surface Science 603 (6) (2009) 852–859. doi:10.1016/j.susc.2009.01.041.

[40] J. W. Han, L. Li, D. S. Sholl, Density Functional Theory Study of H and CO Adsorption on Alkali-Promoted Mo 2 C Surfaces, Journal of Physical Chemistry C 115 (2011) 6870–6876.

[41] T. Wang, X. Liu, S. Wang, C. Huo, Y.-w. Li, J. Wang, H. Jiao, Stability of β-Mo2C Facets from ab Initio Atomistic Thermodynamics, The Journal of Physical Chemistry C ASAP. doi:10.1021/jp205950x.

[42] J. Kitchin, J. K. Nørskov, M. Barteau, J. G. Chen, Trends in the chemical properties of early transition metal carbide surfaces: A density functional study, Catalysis Today 105 (1) (2005) 66–73. doi:10.1016/j.cattod.2005.04.008.

[43] M. Nagai, H. Tominaga, S. Omi, CO Adsorption on Molybdenum Carbides and Molecular Simulation, Langmuir 16 (26) (2000) 10215–10220. doi:10.1021/la000484c.

[44] H. Tominaga, M. Nagai, Density functional study of carbon dioxide hydrogenation on molybdenum carbide and metal, Applied Catalysis A: General 282 (1-2) (2005) 5–13. doi:10.1016/j.apcata.2004.09.041.

[45] J. Ren, C. Huo, J. Wang, Y. Li, H. Jiao, Surface structure and energetics of oxygen and CO adsorption on α-MoC(0001), Surface Science 596 (2005) 212–221. doi:10.1016/j.susc.2005.09.018.

[46] J. Ren, C. Huo, J. Wang, Z. Cao, Y. Li, H. Jiao, Density functional theory study into the adsorption of CO2, H and CHx (x=03) as well as C2H4 on α-Mo2C(0001), Surface Science 600 (11) (2006) 2329–2337. doi:10.1016/j.susc.2006.03.027.

[47] J. Ren, J. Wang, C.-F. Huo, X.-D. Wen, Z. Cao, S. Yuan, Y. Li, H. Jiao, Adsorption of NO, NO2, pyridine and pyrrole on α-Mo2C(0001): A DFT study, Surface Science 601 (6) (2007) 1599–1607. doi:10.1016/j.susc.2007.01.036.

[48] C. Pistonesi, A. Juan, A. P. Farkas, F. Solymosi, DFT study of methanol adsorption and dissociation on β-Mo2C(001), Surface Science 602 (13) (2008) 2206–2211. doi:10.1016/j.susc.2008.04.039.

[49] X.-R. Shi, J. Wang, K. Hermann, CO and NO Adsorption and Dissociation at the -Mo 2 C (0001) Surface : A Density Functional Theory Study, Journal of Physical Chemistry C 114 (2010) 13630–13641.

[50] C. Pistonesi, A. Juan, A. P. Farkas, F. Solymosi, Effects of potassium on the adsorption of methanol on β-Mo2C(001) surface, Surface Science 604 (11-12) (2010) 914–919. doi:10.1016/j.susc.2010.02.020.

[51] A. S. Rocha, A. B. Rocha, V. T. da Silva, Benzene adsorption on Mo2C: A theoretical and experimental study, Applied Catalysis A: General 379 (1-2) (2010) 54–60. doi:10.1016/j.apcata.2010.02.032.

[52] A. Vojvodic, Steam reforming on transition-metal carbides from density-functional theory, Catalysis Letters. Submitted.

[53] H. Tominaga, M. Nagai, Density functional theory of watergas shift reaction on molybdenum carbide., Journal of Physical Chemistry B 109 (43) (2005) 20415–23. doi:10.1021/jp053706u.

[54] P. Liu, J. A. Rodriguez, Water-gas-shift reaction on molybdenum carbide surfaces: essential role of the oxycarbide., Journal of Physical Chemistry B 110 (39) (2006) 19418–25. doi:10.1021/jp0621629.

[55] H. Tominaga, M. Nagai, Mechanism of thiophene hydrodesulfurization on clean/sulfided β-Mo2C(001) based on density func-

tional theorycis- and trans-2-Butene formation at the initial stage, Applied Catalysis A: General 343 (1-2) (2008) 95–103. doi:10.1016/j.apcata.2008.03.034.
[56] K. Reuter, M. Scheffler, Composition, structure, and stability of RuO2(110) as a function of oxygen pressure, Physical Review B 2 (110). arXiv:0107229v1.
[57] J. Enkovaara, C. Rostgaard, J. J. Mortensen, J. Chen, M. Duak, L. Ferrighi, J. Gavnholt, C. Glinsvad, V. Haikola, H. A. Hansen, H. H. Kristoffersen, M. Kuisma, A. H. Larsen, L. Lehtovaara, M. Ljungberg, O. Lopez-Acevedo, P. G. Moses, J. Ojanen, T. Olsen, V. Petzold, N. a. Romero, J. Stausholm-Møller, M. Strange, G. A. Tritsaris, M. Vanin, M. Walter, B. Hammer, H. Häkkinen, G. K. H. Madsen, R. M. Nieminen, J. K. Nørskov, M. Puska, T. T. Rantala, J. Schiøtz, K. S. Thygesen, K. W. Jacobsen, Electronic structure calculations with GPAW: a real-space implementation of the projector augmented-wave method, Journal of Physics: Condensed Matter 22 (25) (2010) 253202. doi:10.1088/0953-8984/22/25/253202.
[58] B. Hammer, L. Hansen, J. K. Nørskov, Improved adsorption energetics within density-functional theory using revised Perdew-Burke-Ernzerhof functionals, Physical Review B 59 (11) (1999) 7413–7421. doi:10.1103/PhysRevB.59.7413.
[59] T. Epicier, J. Dubois, C. Esnouf, G. Fantozzi, Neutron powder diffraction studies of Transition Metal Hemicarbides M2C(1-x) - II. In-situ High Temperature Study on W2C(1-x) and Mo2C(1-x), Acta Metallurgica 36 (8) (1988) 1903.
[60] J. Haines, J. M. Leger, C. Chateau, J. E. Lowther, Experimental and theoretical investigation of Mo2C at high pressure, Journal of Physics: Condensed Matter 13 (2001) 2447–2454.
[61] L. L. Seigle, C. L. Chang, T. P. Sharma, Free energy of formation of Mo2C and the thermodynamic properties of carbon in solid molybdenum, Metallurgical Transactions A 10 (9) (1979) 1223–1228. doi:10.1007/BF02811977.
[62] H. Li, L. Zhang, Q. Zeng, K. Guan, K. Li, H. Ren, S. Liu, L. Cheng, Structural, elastic and electronic properties of transition metal carbides TMC (TM=Ti, Zr, Hf and Ta) from first-principles calculations, Solid State Communications 151 (8) (2011) 602–606. doi:10.1016/j.ssc.2011.02.005.
[63] F. Abild-Pedersen, J. Greeley, F. Studt, J. Rossmeisl, T. Munter, P. G. Moses, E. Skúlason, T. Bligaard, J. K. Nørskov, Scaling Properties of Adsorption Energies for Hydrogen-Containing Molecules on Transition-Metal Surfaces, Physical Review Letters 99 (1) (2007) 4–7. doi:10.1103/PhysRevLett.99.016105.
[64] A. Muramatsu, T. Tatsumi, H. Tominaga, Active species of molybdenum for alcohol synthesis from carbon monoxide-hydrogen, Journal of Physical Chemistry 96 (3) (1992) 1334–1340. doi:10.1021/j100182a058.
[65] C. Zheng, Y. Apeloig, R. Hoffmann, Bonding and coupling of C1 fragments on metal surfaces, Journal of the American Chemical Society 110 (3) (1988) 749–774. doi:10.1021/ja00211a015.
[66] Q. Ge, M. Neurock, H. A. Wright, N. Srinivasan, A First Principles Study of CarbonCarbon Coupling over the {0001} Surfaces of Co and Ru, Journal of Physical Chemistry B 106 (11) (2002) 2826–2829. doi:10.1021/jp013231g.
[67] J. N. Brønsted, Acid and Basic Catalysis., Chemical Reviews 5 (3) (1928) 231–338. doi:10.1021/cr60019a001.
[68] M. G. Evans, M. Polanyi, Inertia and driving force of chemical reactions, Transactions of the Faraday Society 34 (1938) 11. doi:10.1039/tf9383400011.
[69] J. Sehested, S. Dahl, J. Jacobsen, J. Rostrup-Nielsen, Methanation of CO over Nickel : Mechanism and Kinetics at High H2 / CO Ratios, Journal of Physical Chemistry B 109 (2005) 2432–2438.
[70] S. Wang, B. Temel, J. Shen, G. Jones, L. C. Grabow, F. Studt, T. Bligaard, F. Abild-Pedersen, C. H. Christensen, J. K. Nørskov, Universal Brønsted-Evans-Polanyi Relations for CC, CO, CN, NO, NN, and OO Dissociation Reactions, Catalysis Letters 141 (3) (2010) 370–373. doi:10.1007/s10562-010-0477-y.
[71] J. A. Schaidle, A. C. Lausche, L. T. Thompson, Effects of sulfur on Mo2C and Pt/Mo2C catalysts: Water gas shift reaction, Journal of Catalysis 272 (2) (2010) 235–245. doi:10.1016/j.jcat.2010.04.004.
[72] J. Rostrup-Nielsen, J. K. Nørskov, Step sites in syngas catalysis, Topics in Catalysis 40 (1-4) (2006) 45–48. doi:10.1007/s11244-006-0107-5.
[73] A. Vojvodic, F. Calle-Vallejo, W. Guo, S. Wang, A. Toftelund, F. Studt, J. I. Martínez, J. Shen, I. C. Man, J. Rossmeisl, T. Bligaard, J. K. Nørskov, F. Abild-Pedersen, On the behavior of Brønsted-Evans-Polanyi relations for transition metal oxides., Journal of Chemical Physics 134 (24) (2011) 244509. doi:10.1063/1.3602323.
[74] E. C. Weigert, D. V. Esposito, J. G. Chen, Cyclic voltammetry and X-ray photoelectron spectroscopy studies of electrochemical stability of clean and Pt-modified tungsten and molybdenum carbide (WC and Mo2C) electrocatalysts, Journal of Power Sources 193 (2) (2009) 501–506. doi:10.1016/j.jpowsour.2009.04.020.
[75] C. Klünker, CO stretching vibrations on Pt(111) and Pt(110) studied by sumfrequency generation, Surface Science 360 (1-3) (1996) 104–111. doi:10.1016/0039-6028(96)00638-3.
[76] S. R. Bahn, K. W. Jacobsen, An object-oriented scripting interface to a legacy electronic structure code, Computing in Science & Engineering 4 (2002) 56–66.
[77] S. Saadi, B. Hinnemann, S. Helveg, C. C. Appel, F. Abild-Pedersen, J. K. Nørskov, First-principles investigations of the Ni3Sn alloy at steam reforming conditions, Surface Science 603 (5) (2009) 762–770. doi:10.1016/j.susc.2009.01.018.
[78] M. Bollinger, K. W. Jacobsen, J. K. Nørskov, Atomic and electronic structure of MoS2 nanoparticles, Physical Review B 67 (8) (2003) 1–17. doi:10.1103/PhysRevB.67.085410.

Appendix A. Gibbs Free Energies and Chemical Potentials

Computing surface free energies requires knowledge of the Gibbs free energy (G) and chemical potential (μ) of surfaces and gasses at finite temperatures and pressures. This is accomplished via the equation:

$$\begin{aligned} G_i(T,P) &= N_i\,\mu_i(T,P) \\ &= E_{DFT} + U_{ZPE} + \Delta G_{finite}(T,P) \end{aligned} \tag{A.1}$$

where N_i represents the number of molecules of species i, E_{DFT} is the DFT energy (henceforth the variable E corresponds to the DFT energy), U_{ZPE} is the zero-point vibrational energy ($\sum_i \frac{h\nu_i}{2}$) and ΔG_{finite} is the change in Gibbs free energy due to finite temperature and pressure. ΔG_{finite} is estimated using statistical mechanics. Gasses are assumed to be ideal, and adsorbates are treated using the harmonic approximation where all degrees of freedom are treated as frustrated harmonic vibrations and PV contributions are neglected.

Vibrational modes were estimated using a finite difference approximation of the Hessian matrix where energies were calculated with atoms displaced by ± 0.01 Å in the x,y,and z directions. Moments of inertia of gas molecules were calculated based on the optimized geometries. The vibrational modes of an adsorbate were calculated at a coverage of 0.25 ML and it is assumed that these modes are independent of coverage. Coverage dependent frequency shifts are on the order of 10 cm^{-1} for CO on platinum [75] which is negligible compared to the DFT

error. Thermodynamic properties were calculated from vibrational frequencies using standard statistical mechanical equations evaluated through the thermochemistry module of the Atomic Simulation Environment [76]. The Gibbs free energy values calculated for the gas molecules of interest (H_2,H_2O,CO,CH_4) are within 0.01 eV of the tabulated values from NIST across the temperature range of 300-1300 K.

Appendix B. Surface Energies

Analyzing the most stable surfaces under reaction conditions has been accomplished via the *ab initio* thermodynamics formalism developed previously [56], but the general equations will be reviewed in the context of an Mo_2C surface in contact with an atmosphere containing carbon (C), hydrogen (H), and oxygen (O). The Mo_2C surface is considered to be in equilibrium with an atmosphere at a fixed temperature T and pressure P containing gasses composed of C, H, and O. The gasses have partial pressures p_j where j represents all $C_xH_yO_z$ species present. The gas-phase can thus act as a reservoir for C, H, and O and the system can be described by the total Gibbs free energy $G_{tot}(T, p_j, N_i)$ where N_i represents the number of i=C,H,O atoms in the system. It is assumed that the bulk phonon modes are not significantly perturbed by the presence of the surface or adsorbates, as justified previously for another non-metallic system [56]. With this assumption the total energy can be separated into the free energy of the bulk Mo_2C, the Mo_2C surface free energy, and the free energy of the gas-phase reference with which the surface is in equilibrium.

$$G_{tot} = G_{bulk} + G_{surf} + G_{ref} \tag{B.1}$$

$$G_{surf} = G_{tot} - G_{bulk} - \sum_i \Delta N_i \, \mu_i \tag{B.2}$$

where ΔN_i is the number of additional atoms of i ($N_{i,surf} - N_{i,bulk}$) and μ_i is the reference chemical potential for atomic species i. Substituting Equation A.1 into Equation B.2 and normalizing to the surface area A gives the surface energy which is minimized by the most stable surface.

$$\gamma(T, p_j, \Delta N_i) = \frac{1}{A}[E_{tot} - E_{bulk} + U_{ZPE,ads} + \tag{B.3}$$
$$+\Delta G_{finite,ads} - \sum_{i=C,H,O} \Delta N_i \, \mu_i(T, p_j)]$$

where E_{tot} is the DFT energy of the surface and adsorbates, E_{bulk} is the DFT energy of the bulk, $U_{ZPE,ads}$ is the zero-point energy of adsorbates, and $\Delta G_{finite,ads}$ is the free energy of adsorbates discussed in Section Appendix A. The chemical potentials (μ_i) can be explicitly evaluated using Equation A.1 in conjunction with the formalisms in Section Appendix C, ΔN_i is determined by the stoichiometry of the surface, while T and p_j are dictated by the gas composition, temperature, and pressure. Using Equation B.3 it is possible to determine the surface energy of a surface under a given set of reaction conditions. Given a set of n surfaces it is possible to calculate their surface energies γ_n and the most stable equilibrium surface can be predicted by $min(\gamma_n)$. Furthermore, the relative abundance of a surface at equilibrium can be estimated using a Boltzmann distrubution of the surface energies (infinite slab) or a Wulff construction (finite particles) [40, 41]. The minimum energy surface and relative abundance of surfaces determined using these methods assumes that the only possible surfaces are the set of n surfaces for which γ is calculated, and assumes that the system is in equilibrium. Nevertheless, these formalisms provide a useful tool for extrapolating DFT results to finite conditions and can provide insight into which types of surface terminations will be most prevalent [56].

Appendix C. Reference Energies

The values computed for surface and adsorption energies are highly dependent upon the gas-phase reference energies selected. For the systems studied here all adsorbates and non-stoichiometric surfaces contain C, H, and O atoms, and the reactions of interest include H_2, H_2O, CO_x, C_xH_y, and $C_xH_yO_z$ as products and reactants. The relevant reference energy will depend upon the source of the adsorbed species. In the case of atomic hydrogen this is straightforward since molecular hydrogen is a stable molecule that can be easily dissociated according to:

$$H_2 \rightleftharpoons 2H* \tag{C.1}$$
(hydrogen dissociation)

Based on this the energy of H is given by $\frac{1}{2}G_{H_2}$.

Oxygen can be deposited by any of the following reactions:

$$H_2O \rightleftharpoons H_2 + O* \tag{C.2a}$$
(water decomposition)
$$CO_2 \rightleftharpoons CO + O* \tag{C.2b}$$
(CO_2 decomposition)
$$CO \rightleftharpoons CH_4 + O* \tag{C.2c}$$
(CO methanation)
$$O_2 \rightleftharpoons 2O* \tag{C.2d}$$
(oxygen dissociation)

For the conditions of interest in this study the first reaction is most favorable and is expected to be kinetically facile [77]. Assuming this deposition reaction, the reference energy of O is given by G_{H_2O} - G_{H_2}.

Carbon can be deposited by many reactions including:

$$CO + H_2 \rightleftharpoons H_2O + C* \quad \text{(C.3a)}$$
(syngas deposition)
$$C_{graphite} \rightleftharpoons C* \quad \text{(C.3b)}$$
(graphite adsorption)
$$2CO \rightleftharpoons CO_2 + C* \quad \text{(C.3c)}$$
(CO disproportionation)
$$CH_4 \rightleftharpoons 2H_2 + C* \quad \text{(C.3d)}$$
(methane cracking)
$$C_xH_y \rightleftharpoons C_{(x-1)}H_{(y-2)} + H_2 + C* \quad \text{(C.3e)}$$
(hydrocarbon cracking)

Of these reactions the most straightforward is graphite adsorption; however, this is only valid for surfaces covered in graphite which are likely not active for catalysis. When CO is the carbon source the reaction kinetics will depend on CO dissociation, which is an activated process on Mo_2C (as shown in Section 3.3). Methane cracking requires four dehydrogenation steps and is less thermodynamically favorable. Hydrocarbon cracking assumes the presence of higher hydrocarbons in the gas-phase, and also requires multiple steps, including C-C bond breaking.

These considerations imply that the carbon source will change as a function of temperature, pressure, and reactant composition. One common approach to this issue is to simply provide results as a function of an abstract carbon chemical potential. The difficulty in such a strategy is determining the range over which this abstract chemical potential will vary. For many systems such as oxides [56] and sulfides [78] the range is estimated by the gas-phase and bulk energies of the compound. However, for carbides in contact with syngas the situation is not as straightforward. The gas-phase carbon reservoir will depend on the thermodynamics and kinetics of reactions C.3. Furthermore, some of these reactions such as C.3a result in gas-phase carbon which is less stable than bulk graphitic carbon. This leads to carbon chemical potentials above the often used upper limit of $\mu_{graphite}$ [39, 40]. For this reason it is considered more useful to present results either in terms of an abstract chemical potential [Figure 2/4(a)] or by assuming a deposition reaction and gas composition and calculating μ explicitly at various conditions [Figure 2/4(b-d)].

After determining a reference energy the surface free energy can be calculated via Equation B.3 and the adsorption free energy can be calculated as:

$$\Delta G_{ads,A} = G_{surf+A} - G_{surf} - G_{A,reference} \quad \text{(C.4)}$$

so that more negative adsorption energies correspond to stronger binding. In some cases ΔG_{finite} and/or U_{ZPE} terms from Equation A.1 are neglected when computing the adsorption energy in order to directly compare to previous results (as noted in the text).